A hierarchical micromechanics model for nonlinear behavior with damage of SMC composites with wavy fiber

Fei-Yan Zhu[1a], Hyoung Jun Lim[1a], Hoil Choi[1] and Gun Jin Yun[*1,2]

[1]*Department of Aerospace Engineering, Seoul National University, Gwanak-gu, Seoul, 08826, Korea*
[2]*Institute of Advanced Aerospace Technology, Seoul National University, Gwanak-gu, Seoul, 08826, Korea*

Abstract. This paper presents a novel hierarchical micromechanics model to simulate Sheet Molding Compound (SMC) composites with wavy fibers. The three-step homogenizations are integrated to calculate the effective properties of SMC chips, layers, and composites, respectively. During homogenization, it has a unique capability of modeling the wavy fibers within fiber chips through a rotational transformation. The orientation and overlapping of the fiber chips caused by the manufacturing process are considered through the proposed multi-site (MS) micromechanics model. Furthermore, J_2 plasticity and Lemaitre-Chaboche ductile damage models are adopted to estimate the nonlinear behavior of SMC composites. The nonlinear behavior of SMC composites is predicted based on the concurrent simulations at each homogenization. The comparison with results from experiments and the literature validates the proposed hierarchical model. Finally, a parametric study investigates the effects of fiber waviness and chip orientation on the effective behavior of SMC composites.

Keywords: fiber waviness; Mori-Tanaka; multiscale modeling; random distribution; sheet molding compound

1. Introduction

As promising composite materials, discontinuous fiber and chip reinforced composites have received increasing attention in the automotive and urban air mobility industries (Okabe *et al.* 2012, Liu *et al.* 2016, Goris *et al.* 2018). Chopped chip-reinforced composites, formed by compression molding as a sheet molding compound (SMC), extend their capabilities in many lightweight engineering applications (Jendli *et al.* 2004, Fette *et al.* 2017, Wu *et al.* 2018). Compared with traditional continuous fiber composites, SMC composites can achieve a good balance between mechanical performance, formability, and manufacturing (Martulli *et al.* 2020). Moreover, it is more suited for complex geometrical structures, such as landing gears or chassis parts.

The initial charge, which is the preform of the SMC composites, is prepared with chopped fiber tows (or strands) distributed randomly in an uncured thermoset resin (Meyer *et al.* 2020). After that, it is compressed in the shape of the final product. Due to the complex flow pattern during the compression molding process, the final molded parts show a spatially varying distribution of fiber

---

Fei-Yan Zhu, Hyoung Jun Lim, Hoil Choi and Gun Jin Yun

chips. Therefore, significant inhomogeneity and anisotropy are commonly observed, leading to uncertainties of mechanical properties and poses a tremendous challenge to predicting SMC composites' behavior in virtual tests (Trauth *et al.* 2017).

Numerous studies have been reported to deal with the heterogeneity of the SMC composites using analytical or computational micromechanics models. Both micromechanics models for SMC composites have been developed to estimate the effective properties of micro/mesostructure by constructing a representative volume element (RVE) (Sun and Vaidya 1996, Zhu *et al.* 2018, Jeong *et al.* 2019, Lim *et al.* 2021). As a computational micromechanics model, the RVE is constructed through the finite element (FE) method. Jiang *et al.* (2007) presented the FE-based RVE model with a single short fiber and discussed the effects of fiber orientation and aspect ratio on the mechanical properties of composites. Based on the short-fiber modeling, Li *et al.* (2017) developed a finite element SMC model with the random fiber orientation. The rotated stiffness tensors of short fibers were calculated by the rotational transformation and then assigned to the SMC FE RVE model. Next, Chen *et al.* (2018) presented a more realistic SMC model through a stochastic reconstruction algorithm to express the undulation of overlapping between fiber chips. The modified random sequential adsorption (RSA) was adopted to the reconstruction algorithm and generated each SMC layer to deal with the overlapped parts. Recently, Sun *et al.* (2021) generated a woven RVE with a finite element method to cope with the overlapping parts of SMC.

On the other hand, the analytical micromechanics model has become promising due to its high computational efficiency and reasonable accuracy (Doghri and Ouaar 2003, Kanouté *et al.* 2009, Roters *et al.* 2010, Lim *et al.* 2020, Shakouri 2021). It has been developed based on Eshelby's theory which is the foundation of the self-consistent and Mori-Tanaka (MT) methods (Pierard *et al.* 2004, Doghri and Tinel 2005). Among them, the MT method is universally utilized in homogenization calculations for effective properties. It was firstly introduced by Mori and Tanaka (1973) based on the internal stress in the matrix, interaction among inclusions, and energy consideration. Qu (1993) and Fisher *et al.* (2003) improved the MT model with interfacial damage and wavy fiber based on the classical MT method. Recently, efforts have been made to improve the micromechanics model by reflecting the microstructural morphology (Koyama *et al.* 2011, García-Macías *et al.* 2017, Fládr *et al.* 2019, Park *et al.* 2020, Yun *et al.* 2021). Notably, various attempts to predict the mechanical properties of SMC composites with the MT have been explored. Anagnostou *et al.* (2018) presented a micromechanics model to study viscoelastic behavior and damage of SMC-hybrid composites based on the MT approach. Görthofer *et al.* (2020) investigated the influence of the presetting parameters through a sensitivity analysis. The parameters include the elastic moduli, volume fraction of the constituents, and the orientation of fiber. They demonstrated the effects of the parameters by constructing a heatmap. Nevertheless, the previous works have a limitation that only fiber chips' orientation was considered in the micromechanics model. Since the SMC composites are manufactured with a high fiber volume fraction, overlapping between fiber chips and wavy fibers within fiber chip are inevitable in the final product. Therefore, the undulation morphology affects the mechanical performance of the SMC composites and is required to consider in the micromechanics model.

In this paper, a novel hierarchical micromechanics model is presented through a multi-step homogenization method. There are three steps for homogenization in terms of fiber chip, SMC layer, and SMC composites. The first homogenization is to model the fiber chips with wavy fibers. The waviness is implemented by a polynomial mathematical expression, a curve-fitting result, and the selected points from the prescribed normal distribution. Next, the second homogenization is to model the fiber chips with direction on a single layer. A rotational transformation is applied to

express the rotated fiber chip. The overlapping between the fiber chips is also considered through multi-site (MS) Mori-Tanaka (MT) modeling. Finally, the third homogenization is introduced by the Rule of Mixtures (ROM) and bonds the individual layers into solid SMC composites. The integration of J_2 flow rule and Lemaitre-Chaboche damage model is achieved to express nonlinear behavior of SMC composites. The effects of fiber waviness and fiber chips' orientation on mechanical performance are evaluated by parametric study. Moreover, the validity of the proposed model is demonstrated by comparing it with the result of the literature.

2. Micromechanics model with Mori-Tanaka model

2.1 Classical Mori-Tanaka model

In this section, the formulations of the classical Mori-Tanaka (MT) model are presented to obtain the effective properties of SMC composites. In multiscale problem, the local strain $\boldsymbol{\varepsilon}$ and the macroscopic global strain $\boldsymbol{E}$ are connected with a global strain concentration tensor $\boldsymbol{A}$ following the Hill (1965)'s expression, as follows

$$\boldsymbol{\varepsilon}(\boldsymbol{x}) = \boldsymbol{A}(\boldsymbol{x}){:}\boldsymbol{E}, \text{ where } \boldsymbol{E} = \frac{1}{V}\int_V \boldsymbol{\varepsilon}\, dV, \tag{1}$$

where $\boldsymbol{x}$ represents the position vector. For inhomogeneous materials, the calculation process of the global strain concentration tensor is challenging. Following the green tensor technique proposed by Willis (1977), the kinematic integral equation under homogeneous Dirichlet boundary condition with Green's function is used.

$$\boldsymbol{\varepsilon}(\boldsymbol{x}) = \boldsymbol{E}^R(\boldsymbol{x}) - \int_V \boldsymbol{\Gamma}(\boldsymbol{x} - \boldsymbol{x}'){:}\delta\boldsymbol{c}(\boldsymbol{x}'){:}\delta\boldsymbol{\varepsilon}(\boldsymbol{x}')dV \tag{2}$$

Here, $\boldsymbol{\varepsilon}(\boldsymbol{x})$ and $\boldsymbol{c}(\boldsymbol{x}')$ indicate the local strain and local effective stiffness tensor, respectively. The reference medium subjected to homogeneous Dirichlet type boundary condition shows the homogeneous strain field $\boldsymbol{E}^R$. $\boldsymbol{\Gamma}(\boldsymbol{x} - \boldsymbol{x}')$ is the Green's function, and the second term is integrated over the RVE volume V. Eq. (2) provides the method to calculate the strain concentration tensor and to introduce interaction tensor $\boldsymbol{T}^{IJ}$. For *I*-th inclusion, Eq. (2) can also be expressed as Eq. (3).

$$\boldsymbol{\varepsilon}^I = \boldsymbol{E}^R - \sum_{J=0}^N \boldsymbol{T}^{IJ}(\boldsymbol{c}^J - \boldsymbol{c}^R){:}\boldsymbol{\varepsilon}^J, \text{ where } \boldsymbol{T}^{IJ} = \frac{1}{V_I}\iint_{V_I,V_J} \boldsymbol{\Gamma}(\boldsymbol{x} - \boldsymbol{x}')dVdV' \tag{3}$$

Vieville *et al.* (2006) presented an iterative method to update the global strain concentration tensor. Here, considering the inclusion theory, we introduce the local strain concentration tensor $\boldsymbol{a}$.

$$\boldsymbol{\varepsilon}(\boldsymbol{x}) = \boldsymbol{a}(\boldsymbol{x}){:}\boldsymbol{E}^R \tag{4}$$

In this equation, $\boldsymbol{a}(\boldsymbol{x})$ is the local strain concentration tensor that relates to the local strain with the strain field in the infinite reference medium ($\boldsymbol{E}^R$). Combining Eq. (1) and (4), the global strain concentration tensor can be expressed as follows:

$$\boldsymbol{A}(\boldsymbol{x}) = \boldsymbol{a}(\boldsymbol{x}){:}(\overline{\boldsymbol{a}})^{-1}, \text{ where } \overline{\boldsymbol{a}} = \frac{1}{V}\int_V \boldsymbol{a}(\boldsymbol{x})dV. \tag{5}$$

In Eq. (5), the notation $(\overline{\cdot})$ indicates volume-averaged values over the corresponding domain. Therefore, the inclusion of the *I*-th phase can be expressed by Eq. (6).

4

Fei-Yan Zhu, Hyoung Jun Lim, Hoil Choi and Gun Jin Yun

$$A^I = a^I : (\overline{a}^I)^{-1} \tag{6}$$

With the assumption that the RVE is composed of N types of reinforcements and a surrounding matrix which is assumed as the reference medium and labeled as a constituent number 0. It is admitted that particulate inclusions can approach the geometry of reinforcements. As a consequence, the composite is made up of (N+1) constituents. The volume fraction of a given I, or family of the same type of inclusions, is denoted by $f_I = V_I/V$. It is inferred that the properties of each constituent are homogeneous inside the constituent. Hence, in the N phases composites, with the Rule of Mixture, the volume-averaged concentration tensor for I-th inclusion can be calculated as follows:

$$(\overline{a}^I)^{-1} = (f_0 a^0 + \textstyle\sum_{I=1}^{N} f_I a^I)^{-1}. \tag{7}$$

Substituting Eq. (7) into Eq. (5), the global strain concentration tensor is approximated as

$$A^0 = a^0 : (\overline{a}^I)^{-1} = (\overline{a}^I)^{-1} \text{ , where } a^0 = I, \tag{8}$$

where I is the fourth-order identity tensor. Therefore, Eq. (6) can be expressed as Eq. (9).

$$A^I = a^I : (\overline{a}^I)^{-1} = a^I : A^0 \quad \text{with } I=1, 2, \ldots, N \tag{9}$$

The average inclusion strain ($\overline{\varepsilon}^I$) comprise of the perturbed inclusion strain ($\varepsilon^{I^{pt}}$) and the average matrix strain ($\overline{\varepsilon}^0$), as follows,

$$\overline{\varepsilon}^I = \overline{\varepsilon}^0 + \varepsilon^{I^{pt}} = \overline{\varepsilon}^0 + S : \varepsilon^{I^*}. \tag{10}$$

Here, ε^{I^*} is the fictitious eigenstrain of inclusion in V. S is the uniform fourth-order Eshelby tensor of inclusions. Hence, the stress of I-th inclusion can be calculated by

$$\overline{\sigma}^I = c^I : \overline{\varepsilon}^I = c^R : (\overline{\varepsilon}^I - \varepsilon^{I^*}), \tag{11}$$

where c^R and c^I indicate the elastic stiffness tensor of matrix resin and inclusion, respectively. Therefore, from Eq. (11), ε^{I^*} is solved by as following form.

$$\varepsilon^{I^*} = -(c^R)^{-1} : (c^I - c^R) : \overline{\varepsilon}^I \tag{12}$$

Then, substituting Eq. (12) into Eq. (10), the local strain concentration tensor for inclusion is expressed in Eq. (13).

$$\overline{\varepsilon}^I = a^I : \overline{\varepsilon}^0$$

$$a^I = [I + T^{II} : (c^I - c^R)]^{-1} : \left[I - \sum_{J=1,J\neq I}^{N} T^{IJ} : (c^J - c^R) : a^J \right] \tag{13}$$

Here, N is the number of inclusion phases. T^{II} and T^{IJ} are the interaction tensors in on-site (OS) and multi-site (MS) versions, respectively. The OS approximation considers only interaction between the surrounding matrix and the single inclusion, while the MS approximation considers all interactions between different types of inclusion. Their general expression is such that

$$T^{IJ} = \frac{1}{V^I} \int_{V^I} \int_{V^J} \Gamma(r - r') dV dV'. \tag{14}$$

This interaction tensor depends on the assumption on the properties of homogeneous reference medium such as $\mathbf{c}^R$ and $\mathbf{E}^R$. In the case of Mori-Tanaka theory, $\mathbf{c}^R = \mathbf{c}^0$ and $\mathbf{E}^R = \boldsymbol{\varepsilon}^0$ are assumed. In the case of OS approximation, the interaction tensor $\mathbf{T}^{IJ} = 0$, neglecting the interaction between inclusion I and J. The interaction tensor $\mathbf{T}^{II}$ can be deduced from Eshelby's tensor $\mathbf{S}$ such as $\mathbf{T}^{II} = \mathbf{S}:(\mathbf{c}^R)^{-1}$.

Finally, with known Eshelby tensor and strain concentration tensor, the effective stiffness of composites with MT homogenization can be expressed as follows:

$$\overline{\mathbf{C}}^{MT} = \sum_{I=0}^{N} f_I \mathbf{c}^I : \mathbf{A}^I$$

$$= \left(f_0 \mathbf{c}^0 + \sum_{I=1}^{N} f_I \mathbf{c}^I : \mathbf{a}^I \right) : \mathbf{A}^0 \tag{15}$$

$$= \left(f_0 \mathbf{c}^0 + \sum_{I=1}^{N} f_I \mathbf{c}^I : \mathbf{a}^I \right) : \left(f_0 \mathbf{a}^0 + \sum_{I=1}^{N} f_I \mathbf{a}^I \right)^{-1}.$$

2.2 Ductile damage plasticity constitutive model

In this section, a damage plasticity model is introduced to simulate the plastic behavior of polymeric resin with damage. A flow rule is applied to the plasticity model. Stresses are updated at every strain increment, whereas the tangent operator is updated in the plastic domain. By Newton Raphson's method, plastic and damage variables are iteratively updated in the damage plasticity model following the plasticity and ductile damage theory referred to the Lemaitre Chaboche method (Lemaitre 1985). When the resin enters into the plastic regime, the strain is divided into two parts: elastic and plastic strains, as follows,

$$\varepsilon_{ij} = \varepsilon_{ij}^e + \varepsilon_{ij}^p, \tag{16}$$

where ε_{ij} denotes the total strain tensor, and superscripts "e" and "p" indicate the elastic and plastic parts, respectively. An internal variable D ($0 \leq D < 1$) represents the damage state in the matrix. Any solution variable in a damaged state is denoted by $(\cdot)$ as

$$(\cdot) = (1-D)(\hat{\cdot}), \text{ where } (0 \leq D < 1). \tag{17}$$

For an elastoplastic material that obeys J_2 flow, the von Mises yield function, ϕ is represented as

$$\phi(\hat{\sigma}_e, R(p)) = \hat{\sigma}_{eq} - R(p) - \sigma_{y0}, \tag{18}$$

where σ_{y0} is the yield stress of the resin phase, p is the effective plastic strain, $\hat{\sigma}_{eq}$ is the equivalent stress, and $R(p)$ is the isotropic exponential hardening function of the material. They are defined as follows

$$\sigma_{eq} = \sqrt{\frac{3}{2}\hat{\mathbf{s}}:\hat{\mathbf{s}}}, \text{ where } \hat{\mathbf{s}} = \hat{\boldsymbol{\sigma}} - \frac{1}{3}tr(\hat{\boldsymbol{\sigma}})$$

$$R(p) = hp^m, \text{ where } p = \frac{r}{1-D} \tag{19}$$

Here, h and m are parameters associated with isotropic hardening in the form of power laws; and $\boldsymbol{s}$ is the deviatoric stress. In this paper, isotropic hardening is only considered because the significant interest is the expansion and contraction behavior of the yield surface during plastic deformation. If $\phi < 0$, the behavior remains elastic. On the other hand, if $\phi > 0$, then $\dot{p}$ is positive and the plastic strain tensor increment obeys the normal plastic flow, which is summarized by

$$\dot{\varepsilon}^p = \dot{p}\boldsymbol{N}, \text{ where } \boldsymbol{N} = \frac{\partial \phi}{\partial \hat{\sigma}} = \frac{3}{2}\frac{\hat{s}}{\hat{\sigma}_{eq}} \text{ and } \dot{p} = \sqrt{\frac{3}{2}\dot{\varepsilon}^p : \dot{\varepsilon}^p}, \tag{20}$$

where $\boldsymbol{N}$ is the normal vector to the yield surface in the effective stress space. In this formulation, the internal variable p stands for the accumulated plastic strain. In a damaged state, the constitutive relationship is expressed as

$$\boldsymbol{\sigma} = (1-D)\boldsymbol{C} : (\boldsymbol{\varepsilon} - \boldsymbol{\varepsilon}^p). \tag{21}$$

The evolution of the damage is associated with $\dot{p}$ in the Lemaitre-Chaboche model

$$\dot{D} = \begin{cases} 0 & if \ p \leq p_c \\ \left(\dfrac{Y}{S_0}\right)^s \dot{p} & if \ p > p_c \end{cases} \tag{22}$$

In this expression, p_c is a plastic threshold for the evolution of damage, which is prescribed as zero in this paper. In other words, the onset of damage occurs when plastic deformation is initiated. The damage variables are defined as

$$y = \left(\frac{Y}{S_0}\right)^s, \qquad Y = \frac{1}{2E}\left(\frac{\hat{\sigma}_{eq}}{1-D}\right)^2 R_v$$

$$R_v = \frac{2}{3}(1+v) + 3(1-2v)\left[\frac{\hat{\sigma}_H}{\hat{\sigma}_{eq}}\right]^2, \hat{\sigma}_H = \frac{\hat{\sigma}_{kk}}{3}, \tag{23}$$

where S_0 and s are material parameters and $\hat{\sigma}_H$ is the hydrostatic pressure. This section derives an iterative stress update algorithm for the matrix phase used in elastic and plastic regimes. The micro stress update is related to hardening and ductile damage. More details regarding algorithmic tangent operator and stress updating using radial mapping scheme can be found in the literature (Lim *et al.* 2020, Yun *et al.* 2021).

2.3 Integration of ductile damage plasticity model with Mori-Tanaka

In this paper, the ductile damage plasticity constitutive model introduced in Section 2.2 is integrated into the classical Mori-Tanaka model. Fig. 1 shows the overall algorithmic procedures of the Mori-Tanaka homogenization method with ductile damage plasticity model for one-site (OS) and multi-site (MS) models.

Depending on the global strain concentration tensor $\boldsymbol{A}^I$, the local strain increment ($\Delta\boldsymbol{\varepsilon}$) applied differently to the matrix, and inclusion phases are determined as follows

$$\Delta\boldsymbol{\varepsilon}^I = \boldsymbol{A}^I : \Delta\boldsymbol{E}$$

$$\Delta\boldsymbol{\varepsilon}^0 = \frac{\Delta\boldsymbol{E} - f_I\Delta\boldsymbol{\varepsilon}^I}{1-f_I} \tag{24}$$

(a) One-site model ($I = 1$) (b) Multi-site model ($I = 1 \sim N$)
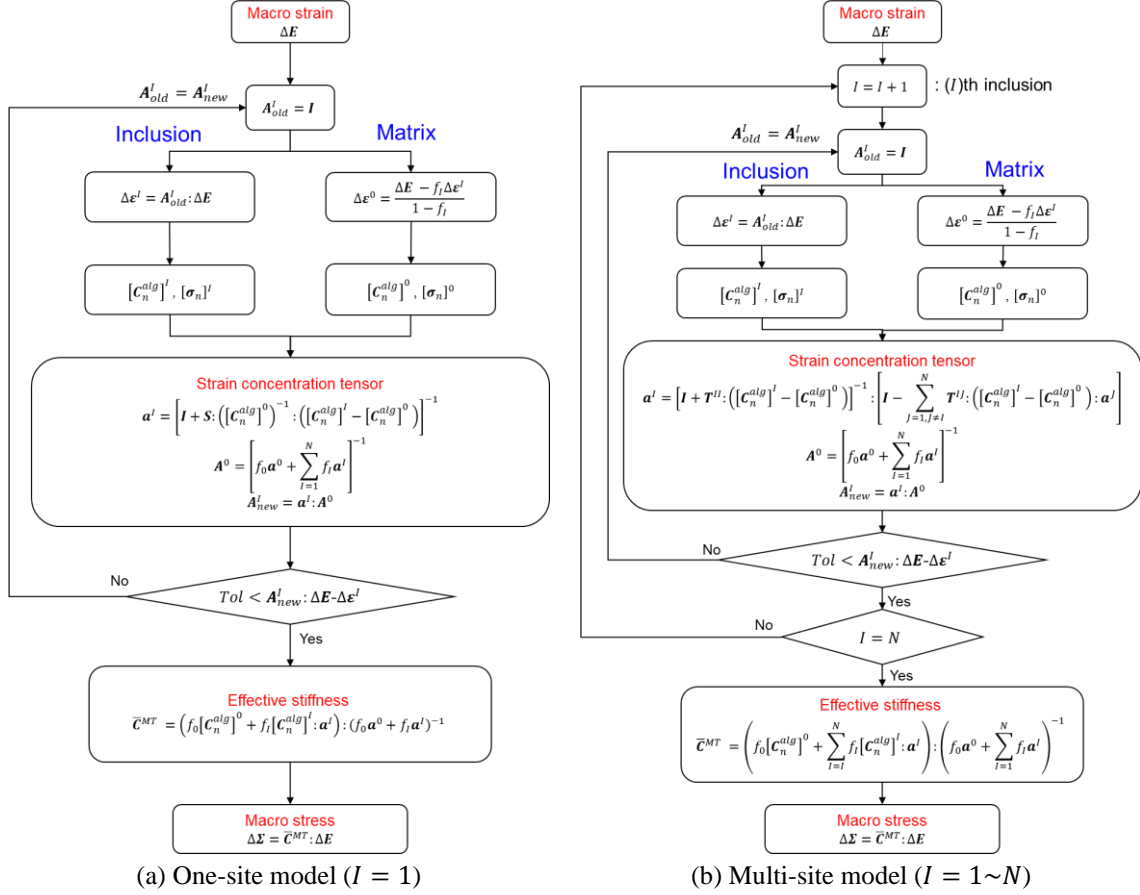
Fig. 1 Flowchart of ductile damage plasticity model with Mori-Tanaka micromechanics

The constituents' algorithmic tangent operator ($\boldsymbol{C}_n^{\text{alg}}$) and stresses ($\boldsymbol{\sigma}_n$) at *n*-th increment state are computed with the local strains. The flow rule judges whether constituents are under a plastic regime or not. The Newton iteration converges the internal variables and calculates each constituent's algorithmic tangent operator and stresses for nonlinear behavior. The only tangent operators of constituents are transferred to the calculation of the local strain concentration tensor ($\boldsymbol{a}^I$). And then, it updates the global strain concentration tensor ($\boldsymbol{A}_{\text{new}}^I$). When the difference between the averaged inclusion strains ($Tol < \boldsymbol{A}^I : \Delta \boldsymbol{E} - \Delta \boldsymbol{\varepsilon}^I$) does not satisfy the criterion, the algorithm goes back to the initial step after updating the global strain concentration tensor ($\boldsymbol{A}_{\text{old}}^I = \boldsymbol{A}_{\text{new}}^I$). The micromechanics model can be divided into OS and MS models depending on the number of inclusions. While the OS model can calculate the homogenized effective stiffness at once, the MS model requires an iterative calculation for tangent operators and the strain concentration tensors for the given number of inclusion types. As a result, the incremental macro stresses of composites are calculated through homogenized effective stiffness.

3. A hirerachical micromechanics model for SMC composites

8

Fei-Yan Zhu, Hyoung Jun Lim, Hoil Choi and Gun Jin Yun

(a) First homogenization: homogenized fiber chips

(b) Second homogenization: homogenized SMC individual layers

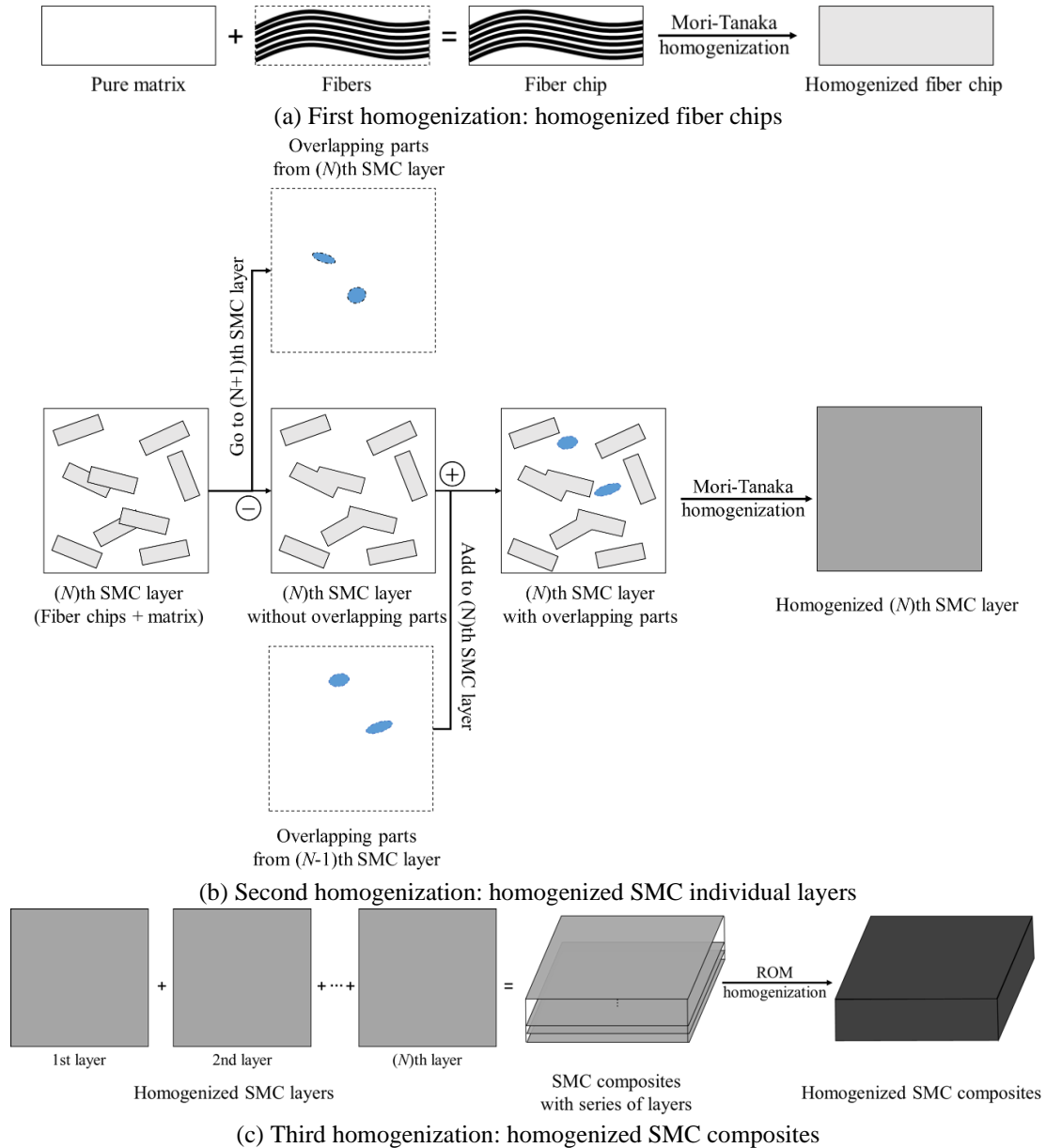(c) Third homogenization: homogenized SMC composites

Fig. 2 The procedure for the proposed multi-homogenization method

A series of multi-step homogenization propose a hierarchical micromechanics model. During the compression molding process, fiber chips are heterogeneously dispersed in the SMC composites with overlapping. In particular, the overlapping between fiber chips could significantly influence the mechanical properties of the composites. The multi-step homogenization method proposed in this section can realize such real-life mesostructure morphology with computational efficiency.

There are three steps for evaluating the effective behavior of SMC composites. The first homogenization step is to model individual fiber chips with wavy fiber. The second homogenization
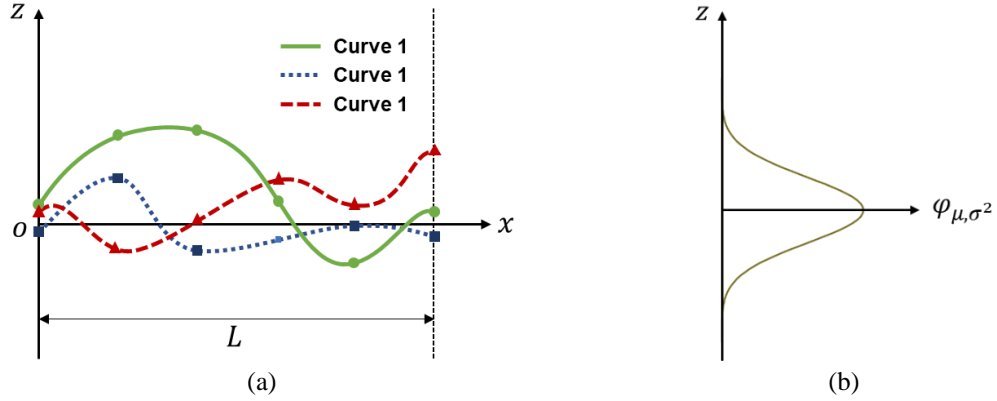
Fig. 3 (a) Randomly wavy fibers, (b) Probability function of a z-coordinate value
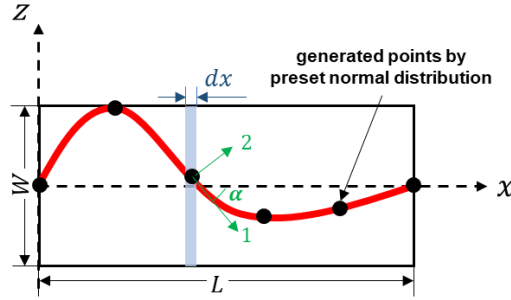

Fig. 4 Representation of random fiber waviness

step is to model a unit SMC layer comprising the randomly oriented fiber chips and resin. The third homogenization step is performed based on the Rule of Mixtures (ROM) to estimate the effective properties of the final SMC composite. The schematic flows for multi-step homogenization are depicted in Fig. 2.

3.1 First homogenization: Modeling fiber chip with wavy fibers

The first homogenization models a chip with wavy fibers by the OS MT method. The projection length of fiber on the *x*-axis is firstly designated to express the wavy fibers in the chips. By generating *z*-coordinate values for the locations along the *x*-axis, the wavy fiber can take any arbitrary shape on the *x-z* plane.

In Fig. 3, three wavy fibers are exhibited by the same fiber projection length L with six points. These are made of equidistant *x*-coordinate values and arbitrary *z*-coordinate values. The arbitrary *z*-coordinate values are determined by random sampling from a preset normal distribution. Therefore, a standard derivation of the normal distribution can control the degree of fibers' waviness. As the standard derivation increases, the waviness of the fiber becomes more random. For the straight fiber, the standard deviation of the normal distribution is set to zero.

As shown in Fig. 4, a fiber is assumed to lie on the *x-z* plane. L and W indicate the length and width of fiber chips, respectively. The wavy fiber is in a polynomial mathematical expression, $z(x) = ax^3 + bx^2 + cx + d$. The coefficients are determined by curve-fitting. It is necessary to
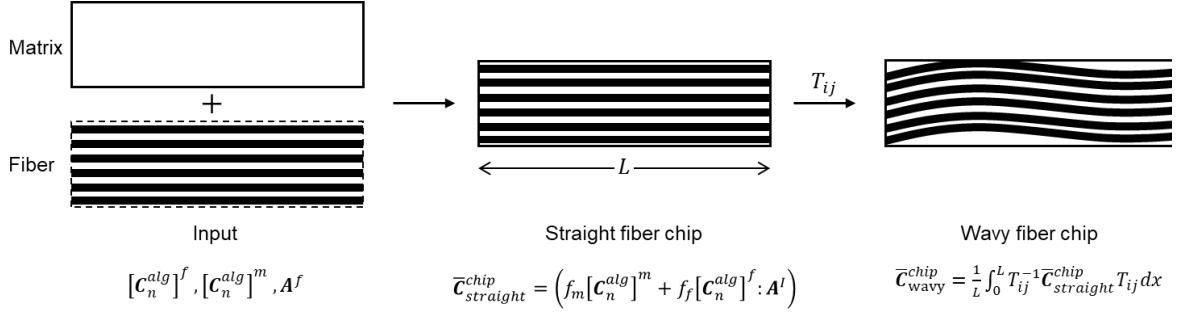
Fig. 5 The micromechanics modeling of wavy fiber chip

calculate the gradient along the x-axis. An analytical differentiation determines the gradient along with the wavy fiber.

From the global to local coordinates system, the stress and strain tensors are converted through a rotational transformation tensor $[T_{ij}]$, as follows

$$\begin{bmatrix} \sigma_{xx} \\ \sigma_{yy} \\ \sigma_{zz} \\ \tau_{yz} \\ \tau_{xz} \\ \tau_{xy} \end{bmatrix} = [T_{ij}]^{-1} \begin{bmatrix} \sigma_{11} \\ \sigma_{22} \\ \sigma_{33} \\ \tau_{23} \\ \tau_{13} \\ \tau_{12} \end{bmatrix}, \quad \begin{bmatrix} \varepsilon_{xx} \\ \varepsilon_{yy} \\ \varepsilon_{zz} \\ \gamma_{xy} \\ \gamma_{xz} \\ \gamma_{xy} \end{bmatrix} = [T_{ij}]^{-1} \begin{bmatrix} \varepsilon_{11} \\ \varepsilon_{22} \\ \varepsilon_{33} \\ \gamma_{23} \\ \gamma_{13} \\ \gamma_{12} \end{bmatrix} \tag{25}$$

$[T_{ij}]$ is expressed using fiber angle α, which is expressed as

$$T_{ij} = \begin{bmatrix} m^2 & 0 & n^2 & 0 & 2mn & 0 \\ 0 & 1 & 0 & 0 & 0 & 0 \\ n^2 & 0 & m^2 & 0 & -2mn & 0 \\ 0 & 0 & 0 & m & 0 & -n \\ -mn & 0 & mn & 0 & m^2 - n^2 & 0 \\ 0 & 0 & 0 & n & 0 & m \end{bmatrix}, \text{where } m = \cos\alpha \text{ and } n = \sin\alpha. \tag{26}$$

As shown in Fig. 2, the angle α is determined by the derivative of $z(x)$. Using the line integral with $[T_{ij}]$, the stiffness matrix in the global coordinates system can be transformed to the local coordinates system as follows

$$\overline{C}_{wavy}^{chip} = \frac{1}{L} \int_0^L T_{ij}^{-1} \, \overline{C}^{MT} T_{ij} dx \tag{27}$$

Here, $\overline{C}^{MT}$ is the effective stiffness of the fiber chip with the unidirectional fiber from Eq. (15), which can also be denoted as $\overline{C}_{straight}^{chip}$. Finally, the stiffness of a single wavy fiber chip is obtained through the rotational transformation expressed in Eq. (27). Fig. 5 illustrates the modeling procedures of the fiber chip. f_m and f_f are the volume fractions of the matrix and fiber, respectively.

3.2 Second homogenization: Modeling unit SMC layer with directional flow and overlapping parts
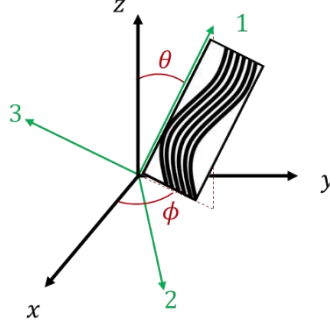
Fig. 6 Defining the angles of fiber chips' orientation

Next, the second MT modeling and homogenization are performed by embedding the fiber chips with the desired orientation into the SMC layer. In the classical Mori-Tanaka homogenization, the fiber chips are aligned to the *x*-axis direction in the global coordinate system. However, in the case of SMC composites manufactured by the compression molding process, the fiber chips could be non-uniformly oriented. Therefore, each layer of SMC composites comprises non-uniformly oriented fiber chips. Effects of such non-uniform orientation on the effective properties of the composites are evaluated through an orientation averaging tensor, which is initially proposed by Odegard *et al.* (2003). The stiffness tensor with the direction of the SMC layer is expressed in Eq. (28)

$$\overline{\boldsymbol{C}}^{layer} = \left(f_0 \boldsymbol{c}^0 + \sum_{I=1}^{N} f_I \langle \boldsymbol{c}^I : \boldsymbol{a}^I \rangle \right) : \left(f_0 \langle \boldsymbol{a}^0 \rangle + \sum_{I=1}^{N} f_I \langle \boldsymbol{a}^I \rangle \right)^{-1} \tag{28}$$

In this equation, the inclusion stiffness ($\boldsymbol{c}^I$) is replaced into $\overline{\boldsymbol{C}}_{wavy}^{chip}$ in Section 3.1. The fiber chips are considered inclusions in the second homogenization for the SMC layer modeling. The notation $\langle \ \rangle$ represents the orientation-averaging tensor computed by Eq. (29), as follows

$$\langle X \rangle_{ijkl} = \frac{\int_0^{\frac{\pi}{2}} \int_{-\pi}^{\pi} X'_{ijkl}(\phi,\theta)\lambda(\theta)sin\theta d\phi \, d\theta}{\int_0^{\frac{\pi}{2}} \int_{-\pi}^{\pi} \lambda(\theta)sin\theta d\phi \, d\theta}, \tag{29}$$

where $\lambda(\theta)$ is the function of θ. X'_{ijkl} is the transformed tensor from the local to global coordinate systems. X'_{ijkl} is defined in Eq. (30)
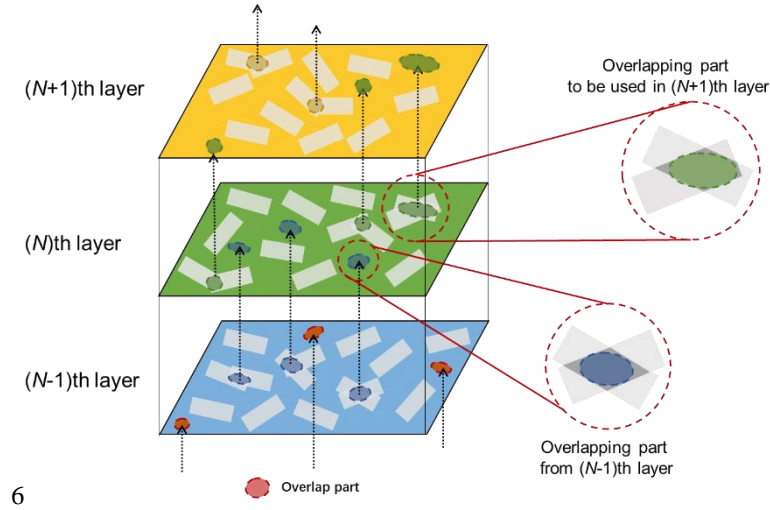
$$X'_{ijkl} = t_{ip}t_{jq}t_{kr}t_{ls}X_{pqrs}$$
$$, \text{where } \boldsymbol{t} = \begin{bmatrix} \cos\theta & -\sin\theta & 0 \\ \sin\theta\cos\phi & \cos\theta\cos\phi & -\sin\phi \\ \sin\theta\sin\phi & \cos\theta\sin\phi & \cos\phi \end{bmatrix}, \tag{30}$$

Here, ϕ and θ are the azimuthal and polar angles denoted in Fig. 6.
To express the random orientation of the fiber chips, $\lambda(\theta)$ is assumed to follow Eq. (31)

$$\lambda(\theta) = e^{-k\theta^2} \tag{31}$$

As k decreases to zero, the fiber chips are randomly oriented. On the other hand, when the k

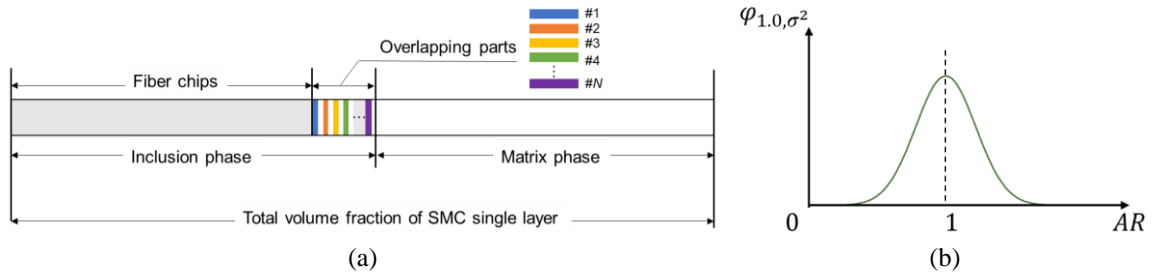Fig. 7 Overlapping parts of chips and mapping to the upper layer

Fig. 8 (a) The contents of SMC composites (b) the normal distribution in terms of aspect ratio (AR) for overlapping parts

diverges to an infinite value, fiber chips become aligned in the x-axis direction. Thus, the fiber chips' orientation changes with $\lambda(\theta)$. The manufacturing process naturally makes randomly distributed fiber chips.

The orientation of fiber chips and the overlapping between fiber chips occur due to the high volume fraction during the compression molding process. Since the SMC layer is set to one unit depth, as shown in Fig. 7, the overlapping parts from the lower layer are considered existent inclusions in the current layer.

In this paper, the overlapping parts are assumed individual ellipsoidal inclusions. Therefore, the shape of overlapping parts is defined by a diameter and aspect ratio. As shown in Fig. 8(a), there are many overlapping parts because of the high volume fraction of the SMC composites. Therefore, the realization of an overlapping part, defined as an arbitrary size, is achieved in the micromechanics model. Because the shape of the overlapping parts is unpredictable, the aspect ratio is assumed to follow the normal distribution, as shown in Fig. 8(b). The SMC layer modeling uses the multi-site (MS) MT model because the overlapping parts are considered ellipsoidal inclusions with different sizes.

A suitable volume fraction of the overlapping phases should be determined for the MS MT modeling. The 20 trials with a 10% overlapping volume fraction of the MS-MT model are computed

A hierarchical micromechanics model for nonlinear behavior with damage of SMC…
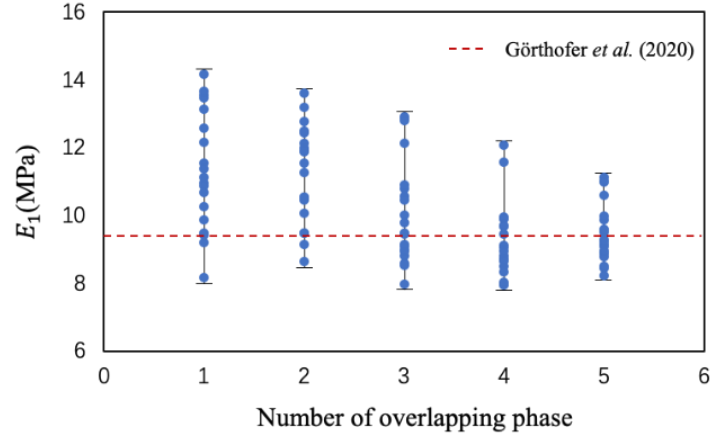

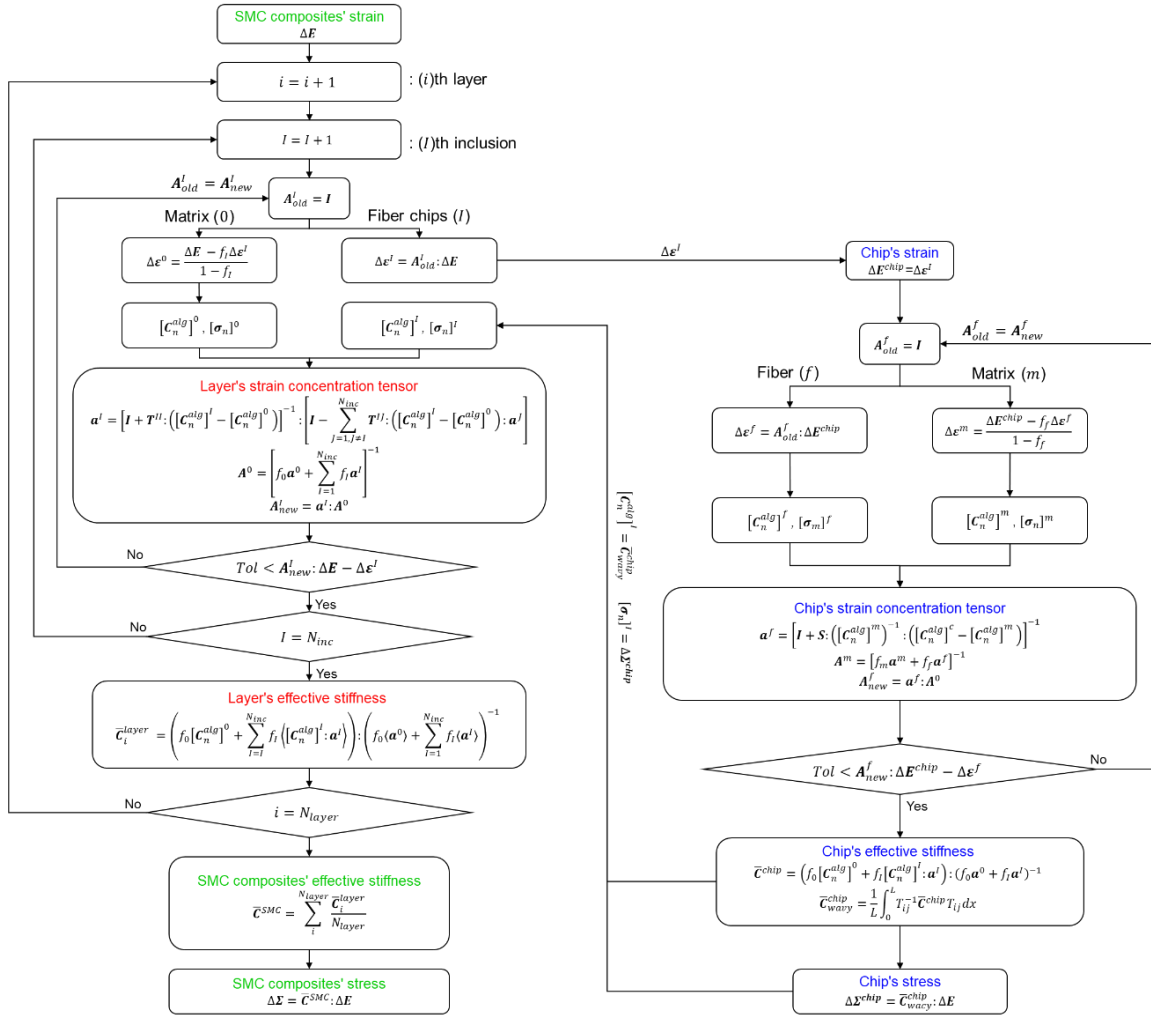Fig. 9 Effect of the number of overlapping phases on the effective elastic modulus

Fig. 10 Flowchart of multi-step homogenization

for the elastic modulus. The 20 trial simulations use the parameters in Section 4.1. The results are then compared with that of Görthofer *et al.* (2020). As shown in Fig. 9, when the overlapping phases are insufficient, the calculated modulus is slightly larger than the value in the literature. Moreover, the variance of modulus appears to be gradually converged as the number of overlapping phases increases. Given that a large number of phases lead to tremendous computational time, the number of overlapping phases is set to be five, which satisfies both validity and computational efficiency.

3.3 Third homogenization: Combining SMC layers using ROM

Finally, the effective properties of the SMC composites are obtained through the Rule of the mixtures (ROM) with virtual layer-by-layer laminations. The homogenized unit SMC layers are laminated into an SMC solid composite. Depending on the preset variables, SMC layers have different homogenized properties calculated in the second homogenization. The effective stiffness of SMC composites is expressed with the homogenized unit layers' stiffnesses, as follows

$$\overline{\boldsymbol{C}}^{SMC} = \sum_{i}^{N_{layer}} \frac{\overline{\boldsymbol{C}}_{i}^{layer}}{N_{layer}} \tag{32}$$

where N_{layer} is the total number of layers. In Eq. (32), because the layers constituting the SMC composite are assumed to have the same thickness, the volume fraction of each layer is $1/N_{layer}$. As a result, the average value of layers' effective stiffness is the effective stiffness of the SMC composites.

The multi-step homogenization for SMC composites is summarized in Fig. 10. The OS and MS models of the MT method are utilized on the fiber chip and SMC layer, respectively. And then, the Rule of Mixtures (ROM) is applied to calculate the effective stiffness of SMC composites. This algorithm starts from the strain increment of SMC composites. The SMC composites' strain is divided into phases of matrix and fiber chips. Furthermore, the strain of fiber chips is once more separated into the matrix and fiber phases. The first homogenization is conducted based on the material properties of fiber and matrix. The effective stiffness and stress of the fiber chip with wavy fibers are transferred to the second homogenization. The effective stiffness of the SMC layer is constructed based on the orientation averaging tensor owing to non-uniformly distributed fiber chips. During the second homogenization, overlapping parts are simultaneously considered by assuming ellipsoidal inclusions. The final step is to obtain the effective stiffness of SMC composites through ROM. The simulations at each stage are concurrently performed because ductile damage plasticity of the matrix is applied to the matrix phase. As an input, the strain increment of SMC composites is entered into this algorithm. Through the multi-step homogenization, the stress increment of SMC composites is calculated as output.

4. Numerical simulation results and discussion

4.1 Model validation with the literature

The proposed hierarchical micromechanics model is validated with the results from the literature. Görthofer *et al.* (2020) developed a rapid microstructure generator of SMC composites through closure approximations for the fiber orientation tensor. They utilized E-glass fiber and unsaturated

Table 1 Material parameters of fiber chips (Kehrer *et al.* 2018)

	E-glass fibers	UPPH matrix
Young's Modulus (GPa)	72	3.4
Shear Modulus (GPa)	29.51	1.23
Poisson ratio	0.22	0.385

Table 2 Results comparison of fiber chip

	Görthofer *et al.* (2020)	Presented method
E_L (GPa)	37.73	38.75
E_T (GPa)	10.33	10.61
G_L (GPa)	3.58	4.87
G_T (GPa)	3.64	4.87
v_L	0.477	0.489
v_T	0.292	0.318

Table 3 Comparison of effective elastic properties of SMC composites for the proposed method and literatures

	Görthofer *et al.* (2020)	Trauth *et al.* (2017)	Kehrer *et al.* (2018)	Proposed method
E_x (GPa)	9.42	10.96±0.3	10.92±0.6	9.88±0.5
E_y (GPa)	8.21	9.25±1.0	8.28±0.5	7.46±0.6
E_z (GPa)	6.19			7.46±0.6
G_{yz} (GPa)	1.95			3.02±0.5
G_{xz} (GPa)	1.96			3.02±0.5
G_{xy} (GPa)	3.11			3.43±0.4
v_{yz}	0.398			0.398±0.1
v_{xz}	0.368			0.385±0.1
v_{xy}	0.342			0.385±0.1

polyester polyurethane hybrid (UPPH) resin for fiber chips. The material properties are summarized in Table 1.

They used numerical full-field homogenization of a representative fiber chip. Fiber chips consisting of approximately 225 aligned continuous fibers with a diameter of approximately 13.5 μm are cut to a 25.4 mm length. A fiber volume fraction within a fiber chip is set to 50%. The comparison on elastic properties, with "*L*" standing for longitudinal and "*T*" for transverse direction, are summarized in Table 2.

All the material properties reasonably match with results from the literature. And then, the elastic properties of SMC composites are evaluated and also compared with the literature. Görthofer *et al.* (2020) constructed the SMC model with fiber chips. The size of fiber chips is designed 50 mm×5 mm and distributed in 250 mm×250 mm plate with seven layers. The orientation tensor is determined through μ-CT (Computed Tomography) scans and image processing. The resulting effective orthotropic engineering properties are collected in Table 3.

In the proposed model, for imitating the orientation tensor in the literature, fiber chips are distributed in a matrix with an orientation variable k=0.32, and the number of layers is assumed to be 20. The number of overlapping types is set to be five (six types of inclusions, including SMC chips) with a 10% volume ratio in the total fiber volume. With the 50% chips' volume fraction in

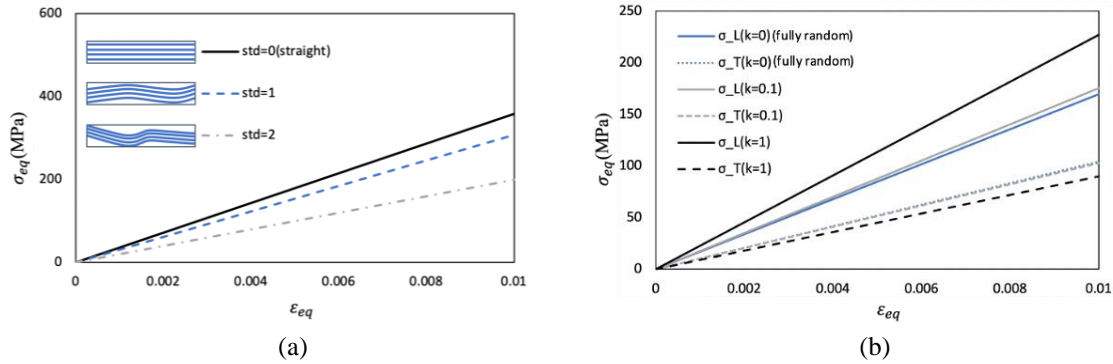*Fei-Yan Zhu, Hyoung Jun Lim, Hoil Choi and Gun Jin Yun*

Fig. 11 The stress-strain curves (a) the influence of the waviness on SMC chip and (b) the influence of the orientation on SMC composites
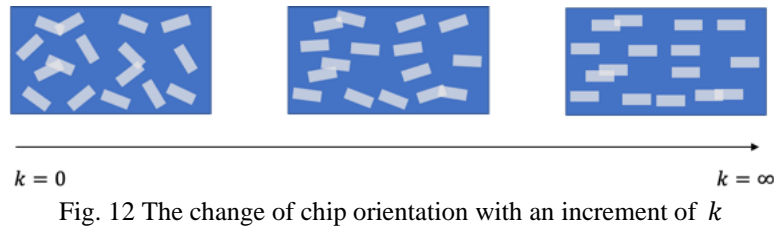

Fig. 12 The change of chip orientation with an increment of k

each layer, the fiber volume fraction of 25% is achieved in this comparison. The variance of the material properties is obtained out of ten trials with the randomness of the waviness (*std*=1). The proposed method is compared with experiments and the literature with high accuracy, demonstrating the proposed method's validity. The slight difference may be attributed to waviness and orientation effects that cannot coincide precisely with the experiments and the literature.

4.2 Effect of waviness and orientation

The manufacturing-dependent fibers' waviness and chips' orientation greatly influence on elastic properties of the SMC composites. In this section, the effect of fibers' waviness within chips is investigated through a case study. For micromechanics modeling, the material properties of constituents in Table 1 are assumed, and a monotonic loading is applied in the longitudinal direction. Wavy fibers are set as explained in Section 3.1 and classified into three cases. The stress-strain responses of fiber chips are summarized in Fig. 11(a). The results show that the existence of waviness reduces mechanical properties.

Next, with the increment of the orientation variable k, the longitudinal and transverse stress-strain behavior of the SMC composites are plotted in Fig. 11(b). The anisotropy of SMC composites is expressed by $\lambda(\theta)$ that is a function of k. The schematic tendency of anisotropy is depicted in Fig. 12. The behavior in the longitudinal direction becomes stiffer as fiber chips are aligned to the corresponding direction. When fiber chips are randomly distributed, the elastic behavior along the *x* and *y* directions becomes similar. The parametric study demonstrates that the waviness and orientation are critical parameters determining the elastic behavior of both fiber chips and SMC composites. Further study is conducted by calculating the nonlinear behavior of SMC composites under cyclic loading.

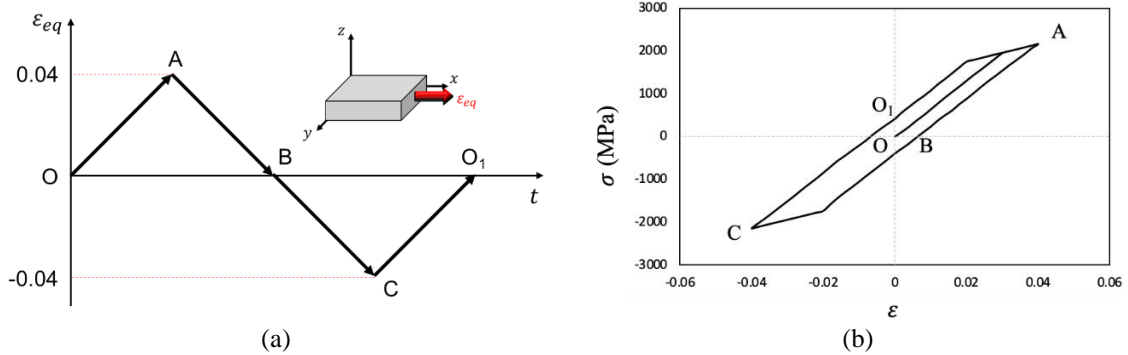(a)   (b)

Fig. 13 Cyclic loading condition and the response of SMC composites: (a) Cyclic loading condition (b) cyclic stress-strain curve
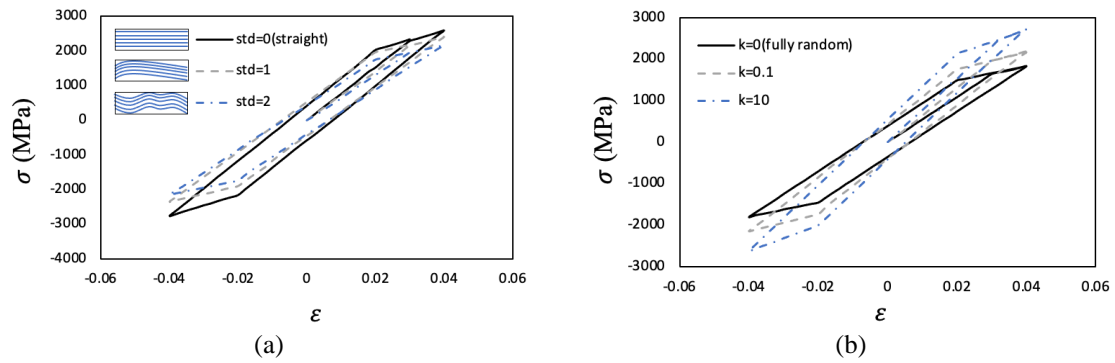

(a)   (b)

Fig. 14 Cyclic stress-strain responses (a) waviness (b) orientation distribution

4.3 The SMC micromechanics model under cyclic loading

In this section, the hierarchical micromechanics model is conducted to obtain the nonlinear behavior of the SMC composites under cyclic loading. The cyclic loading condition is applied to the *x*-axis, as shown in Fig. 13. The strain is cyclic in the interval [-0.04, 0.04]. The amplitude of strain is prescribed so that it reaches a plastic regime for nonlinear behavior.

During the OA loading process, the continuous increment of strain causes plasticity with ductile damage. Once the strain arrives at positive maximum loading point A, the loading strain begins to decrease until the negative maximum loading point C linearly. The response of SMC composites follows the elastic properties until reaching the plastic regime. After that, a hardening slope with ductile damage has appeared. As a result, unrecoverable plastic strain is generated in the compressive loading. In this simulation, CF/PA6 SMC composites are modeled. The material parameters are referred from the literature (Azoti and Elmarakbi 2017, Wan and Takahashi 2020).

Fig. 14(a) indicates the effect of waviness on the cyclic stress-strain responses of SMC composites. The material properties are adopted from Table 1. The volume fraction of fiber and orientation variable k are prescribed as 20% and 0.1, respectively. The fiber chips with three different kinds of waviness are generated through the calculation. Fig. 14(a) shows that the waviness negatively influences both elastic and damage-plastic regimes. Next, Fig. 14(b) shows that the random distribution with k=0 decreases the material properties not only elastic but also damage-

plastic regime. All the models have wavy fibers in the fiber chips with *std*=2. Since the aligned fibers to the loading direction provide enormous elastic and plastic, the randomly distributed fiber chips lead SMC composites to diminish the performance along the loading direction.

5. Conclusions

This paper proposed a novel multi-step homogenization method for SMC composites by considering manufacturing-dependent parameters. Mainly, fibers' waviness and chips' orientation were defined in the micromechanics model through a statistical formulation. The influence of these parameters on the elastic and nonlinear behavior of SMC composites was investigated through the parametric study. Moreover, the proposed method was successfully validated against the literature in the elastic domain. As a result, the following conclusions are derived:

• The manufacturing-dependent parameters were modeled: (1) the waviness followed the coordinate transformation and orientation averaging algorithm. (2) the orientation of fiber chips was realized by integration of the strain concentration tensor.
• A fully implicit updated model was adopted to observe the damage-plastic behavior of the SMC composites.
• The multi-step homogenization algorithm was presented to simulate the SMC composites by considering the manufacturing process. The first step is to homogenize the fiber and matrix into fiber chips; the second step is to homogenize the SMC chips and matrix into the SMC layer; the third step is to homogenize SMC layers into SMC solid composites.
• The overlapping problem of SMC chips was solved by appending extra inclusion phases in the multi-site (MS) Mori-Tanaka (MT) model.
• The simulations on the influences of the waviness and orientation were presented through a parametric study.
• The proposed model had a good agreement with the results from the literature and demonstrated its validity and accuracy.

Acknowledgments

References

Anagnostou, D., Chatzigeorgiou, G., Chemisky, Y. and Meraghni, F. (2018), "Hierarchical micromechanical modeling of the viscoelastic behavior coupled to damage in SMC and SMC-hybrid composites", *Compos. Part B Eng.*, **151**, 8-24. https://doi.org/10.1016/j.compositesb.2018.05.053.
Azoti, W. and Elmarakbi, A. (2017), "Constitutive modelling of ductile damage matrix reinforced by platelets-like particles with imperfect interfaces: Application to graphene polymer nanocomposite materials", *Compos. Part B Eng.*, **113**, 55-64. https://doi.org/10.1016/j.compositesb.2017.01.007.
Chen, Z., Huang, T., Shao, Y., Li, Y., Xu, H., Avery, K., Zeng, D., Chen, W. and Su, X. (2018), "Multiscale finite element modeling of sheet molding compound (SMC) composite structure based on stochastic

mesostructure reconstruction", *Compos. Struct*., **188**, 25-38. https://doi.org/10.1016/j.compstruct.2017.12.039.

Doghri, I. and Ouaar, A. (2003), "Homogenization of two-phase elasto-plastic composite materials and structures: Study of tangent operators, cyclic plasticity and numerical algorithms", *Int. J. Solid. Struct*., **40**(7), 1681-1712. https://doi.org/10.1016/S0020-7683(03)00013-1.

Doghri, I. and Tinel, L. (2005), "Micromechanical modeling and computation of elasto-plastic materials reinforced with distributed-orientation fibers", *Int. J. Plast*., **21**(10), 1919-1940. https://doi.org/10.1016/j.ijplas.2004.09.003.

Fette, M., Hentschel, M., Santafe, J.G., Wille, T., Büttemeyer, H. and Schiebel, P. (2017), "New methods for computing and developing hybrid sheet molding compound structures for aviation industry", *Procedia CIRP*, **66**, 45-50. https://doi.org/10.1016/j.procir.2017.03.289.

Fládr, J., Bílý, P. and Broukalová, I. (2019), "Evaluation of steel fiber distribution in concrete by computer aided image analysis", *Compos. Mater. Eng*., **1**(1), 49-70. https://doi.org/10.12989/cme.2019.1.1.049.

García-Macías, E., Rodríguez-Tembleque, L., Castro-Triguero, R. and Sáez, A. (2017), "Eshelby-Mori-Tanaka approach for post-buckling analysis of axially compressed functionally graded CNT/polymer composite cylindrical panels", *Compos. Part B Eng*., **128**, 208-224. https://doi.org/10.1016/j.compositesb.2017.07.016.

Goris, S., Back, T., Yanev, A., Brands, D., Drummer, D. and Osswald, T.A. (2018), "A novel fiber length measurement technique for discontinuous fiber-reinforced composites: A comparative study with existing methods", *Polym. Compos*., **39**(11), 4058-4070. https://doi.org/10.1002/pc.24466.

Görthofer, J., Schneider, M., Ospald, F., Hrymak, A. and Böhlke, T. (2020), "Computational homogenization of sheet molding compound composites based on high fidelity representative volume elements", *Comput. Mater. Sci*., **174**, 109456. https://doi.org/10.1016/j.commatsci.2019.109456.

Hill, R. (1965), "A self-consistent mechanics of composite materials", *J. Mech. Phys. Solid*., **13**(4), 213-222. https://doi.org/10.1016/0022-5096(65)90010-4.

Jendli, Z., Meraghni, F., Fitoussi, J. and Baptiste, D. (2004), "Micromechanical analysis of strain rate effect on damage evolution in sheet molding compound composites", *Compos. Part A Appl. Sci. Manuf*., **35**(7), 779-785. https://doi.org/10.1016/j.compositesa.2004.01.020.

Jeong, S., Zhu, F., Lim, H., Kim, Y. and Yun, G.J. (2019), "3D stochastic computational homogenization model for carbon fiber reinforced CNT/epoxy composites with spatially random properties", *Compos. Struct*., **207**, 858-870. https://doi.org/10.1016/j.compstruct.2018.09.025.

Jiang, B., Liu, C., Zhang, C., Wang, B. and Wang, Z. (2007), "The effect of non-symmetric distribution of fiber orientation and aspect ratio on elastic properties of composites", *Compos. Part B Eng*., **38**(1), 24-34. https://doi.org/10.1016/j.compositesb.2006.05.002.

Kanouté, P., Boso, D.P., Chaboche, J.L. and Schrefler, B.A. (2009), "Multiscale methods for composites: A review", *Arch. Comput. Method. Eng*., **16**(1), 31-75. https://doi.org/10.1007/s11831-008-9028-8.

Kehrer, L., Wicht, D., Wood, J.T. and Böhlke, T. (2018), "Dynamic mechanical analysis of pure and fiber-reinforced thermoset- and thermoplastic-based polymers and free volume-based viscoelastic modeling", *GAMM-Mitteilungen*, **41**(1), e201800007. https://doi.org/10.1002/gamm.201800007.

Koyama, S., Katano, S., Saiki, I. and Iwakuma, T. (2011), "A modification of the Mori-Tanaka estimate of average elastoplastic behavior of composites and polycrystals with interfacial debonding", *Mech. Mater*., **43**(10), 538-555. https://doi.org/10.1016/j.mechmat.2011.06.010.

Lemaitre, J. (1985), "A continuous damage mechanics model for ductile fracture", *J. Eng. Mater. Tech*., **107**(1), 83-89. https://doi.org/10.1115/1.3225775.

Li, Y., Chen, Z., Xu, H., Dahl, J., Zeng, D., Mirdamadi, M. and Su, X. (2017), "Modeling and simulation of compression molding process for Sheet Molding Compound (SMC) of chopped carbon fiber composites", *SAE Int. J. Mater. Manuf*., **10**(2), 130-137.

Lim, H.J., Choi, H., Lee, M.J. and Yun, G.J. (2021), "An efficient multi-scale model for needle-punched Cf/SiCm composite materials with experimental validation", *Compos. Part B Eng*., **217**, 108890. https://doi.org/10.1016/j.compositesb.2021.108890.

Lim, H.J., Choi, H., Zhu, F.Y., Kerekes, T.W. and Yun, G.J. (2020), "Multiscale damage plasticity modeling

and inverse characterization for particulate composites", *Mech. Mater.*, **149**, 103564. https://doi.org/10.1016/j.mechmat.2020.103564.

Liu, H., Zeng, D., Li, Y. and Jiang, L. (2016), "Development of RVE-embedded solid elements model for predicting effective elastic constants of discontinuous fiber reinforced composites", *Mech. Mater.*, **93**, 109-123. https://doi.org/10.1016/j.mechmat.2015.10.011.

Martulli, L.M., Creemers, T., Schöberl, E., Hale, N., Kerschbaum, M., Lomov, S.V. and Swolfs, Y. (2020), "A thick-walled sheet moulding compound automotive component: Manufacturing and performance", *Compos. Part A Appl. Sci. Manuf.*, **128**, 105688. https://doi.org/10.1016/j.compositesa.2019.105688.

Meyer, N., Schöttl, L., Bretz, L., Hrymak, A.N. and Kärger, L. (2020), "Direct bundle simulation approach for the compression molding process of Sheet Molding Compound", *Compos. Part A Appl. Sci. Manuf.*, **132**, 105809. https://doi.org/10.1016/j.compositesa.2020.105809.

Mori, T. and Tanaka, K. (1973), "Average stress in matrix and average elastic energy of materials with misfitting inclusions", *Acta Metallurgica*, **21**(5), 571-574. https://doi.org/10.1016/0001-6160(73)90064-3.

Odegard, G.M., Gates, T.S., Wise, K.E., Park, C. and Siochi, E.J. (2003), "Constitutive modeling of nanotube-Reinforced polymer composites", *Compos. Sci. Tech.*, **63**(11), 1671-1687. https://doi.org/10.1016/S0266-3538(03)00063-0.

Okabe, T., Motani, T., Nishikawa, M. and Hashimoto, M. (2012), "Numerical simulation of microscopic damage and strength of fiber-reinforced plastic composites", *Adv. Compos. Mater.*, **21**(2), 147-163. https://doi.org/10.1080/09243046.2012.688495.

Park, I., Moon, J., Bae, S., Oh, J.E. and Yoon, S. (2020), "Application of micro-CT to Mori-Tanaka method for non-randomly oriented pores in air-entrained cement pastes", *Constr. Build. Mater.*, **255**, 119342. https://doi.org/10.1016/j.conbuildmat.2020.119342.

Pierard, O., Friebel, C. and Doghri, I. (2004), "Mean-field homogenization of multi-phase thermo-elastic composites: a general framework and its validation", *Compos. Sci. Tech.*, **64**(10), 1587-1603. https://doi.org/10.1016/j.compscitech.2003.11.009.

Roters, F., Eisenlohr, P., Hantcherli, L., Tjahjanto, D.D., Bieler, T.R. and Raabe, D. (2010), "Overview of constitutive laws, kinematics, homogenization and multiscale methods in crystal plasticity finite-element modeling: Theory, experiments, applications", *Acta Materialia*, **58**(4), 1152-1211. https://doi.org/10.1016/j.actamat.2009.10.058.

Shakouri, M. (2021), "Analytical solution for stability analysis of joined cross-ply thin laminated conical shells under axial compression", *Compos. Mater. Eng.*, **3**(2), 117-134. https://doi.org/10.12989/cme.2021.3.2.117.

Sun, C.T. and Vaidya, R.S. (1996), "Prediction of composite properties from a representative volume element", *Compos. Sci. Tech.*, **56**(2), 171-179. https://doi.org/10.1016/0266-3538(95)00141-7.

Sun, Q., Zhou, G., Meng, Z., Jain, M. and Su, X. (2021), "An integrated computational materials engineering framework to analyze the failure behaviors of carbon fiber reinforced polymer composites for lightweight vehicle applications", *Compos. Sci. Tech.*, **202**, 108560. https://doi.org/10.1016/j.compscitech.2020.108560.

Trauth, A., Pinter, P. and Weidenmann, K.A. (2017), "Investigation of quasi-static and dynamic material properties of a structural sheet molding compound combined with acoustic emission damage analysis", *J. Compos. Sci.*, **1**(2), 18. https://doi.org/10.3390/jcs1020018.

Vieville, P., Bonnet, A. and Lipiński, P. (2006), "Modelling effective properties of composite materials using the inclusion concept. General considerations", *Arch. Mech.*, **58**(3), 207-239.

Wan, Y. and Takahashi, J. (2020), "Mechanical modeling of CF/PA6 sheet molding compounds with X-ray computed tomography-based internal geometry considerations", *Compos. Sci. Tech.*, **192**, 108104. https://doi.org/10.1016/j.compscitech.2020.108104.

Willis, J.R. (1977), "Bounds and self-consistent estimates for the overall properties of anisotropic composites", *J. Mech. Phys. Solid.*, **25**(3), 185-202. https://doi.org/10.1016/0022-5096(77)90022-9.

Wu, Y., Xia, C., Cai, L., Garcia, A.C. and Shi, S.Q. (2018), "Development of natural fiber-reinforced composite with comparable mechanical properties and reduced energy consumption and environmental impacts for replacing automotive glass-fiber sheet molding compound", *J. Clean. Prod.*, **184**, 92-100.

https://doi.org/10.1016/j.jclepro.2018.02.257.

Yun, G.J., Zhu, F.Y., Lim, H.J. and Choi, H. (2021), "A damage plasticity constitutive model for wavy CNT nanocomposites by incremental Mori-Tanaka approach", *Compos. Struct*., **258**, 113178. https://doi.org/10.1016/j.compstruct.2020.113178.

Zhu, F.Y., Jeong, S., Lim, H.J. and Yun, G.J. (2018), "Probabilistic multiscale modeling of 3D randomly oriented and aligned wavy CNT nanocomposites and RVE size determination", *Compos. Struct*., **195**, 265-275. https://doi.org/10.1016/j.compstruct.2018.04.060.

CC